Published in final edited form as:
Neuron. 2004 May 27; 42(4): 595–605.

A Highly Ca^{2+}-Sensitive Pool of Vesicles Contributes to Linearity at the Rod Photoreceptor Ribbon Synapse

Wallace B. Thoreson[1,2,*], **Katalin Rabl**[1,5], **Ellen Townes-Anderson**[3], and **Ruth Heidelberger**[4]

[1] Department of Ophthalmology, University of Nebraska Medical Center, Omaha, Nebraska 68198

[2] Department of Pharmacology, University of Nebraska Medical Center, Omaha, Nebraska 68198

[3] Department of Neurology and Neurosciences, University of Medicine and Dentistry-New Jersey, Medical School, Newark, New Jersey 07103

[4] Department of Neurobiology and Anatomy, University of Texas Health Science Center at Houston, Houston, Texas 77030

Summary

Studies of the properties of synaptic transmission have been carried out at only a few synapses. We analyzed exocytosis from rod photoreceptors with a combination of physiological and ultrastructural techniques. As at other ribbon synapses, we found that rods exhibited rapid kinetics of release, and the number of vesicles in the releasable pool is comparable to the number of vesicles tethered at ribbon-style active zones. However, unlike other previously studied neurons, we identified a highly Ca^{2+}-sensitive pool of releasable vesicles with a relatively shallow relationship between the rate of exocytosis and $[Ca^{2+}]_i$ that is nearly linear over a presumed physiological range of intra-terminal $[Ca^{2+}]$. The low-order $[Ca^{2+}]$ dependence of release promotes a linear relationship between Ca^{2+} entry and exocytosis that permits rods to relay information about small changes in illumination with high fidelity at the first synapse in vision.

Introduction

Calcium-dependent release of neurotransmitter during synaptic transmission is a fundamental feature of nervous system function. In the best-characterized peripheral and central neurons, the relationship between the magnitude of Ca^{2+} entry through voltage-gated Ca^{2+} channels and neurotransmitter release is approximately third-order (Dodge and Rahamimoff, 1967; Augustine et al., 1985; Mintz et al., 1995; Borst and Sakmann, 1999; Wu et al., 1999). This has been taken as indirect evidence that neurotransmitter release is triggered by the binding of at least three Ca^{2+} ions to the Ca^{2+} sensor(s) for exocytosis (Dunlap et al., 1995). The highly cooperative nature of neuronal exocytosis is further supported by studies in which the relationship between the concentration of Ca^{2+} near release sites and the rate of exocytosis has been directly ascertained. However, such detailed analysis of the Ca^{2+} sensitivity of the release machinery has only been performed in three neurons to date: the retinal ON bipolar cell, the cochlear hair cell, and the presynaptic neuron at the calyx of Held. Despite profound differences in their physiological properties, each of these neurons demonstrated a fourth- or fifth-order relationship between the presumed Ca^{2+} concentration near release sites and the rate of synaptic vesicle fusion

[*]Correspondence: wbthores@unmc.edu.
[5]On leave from the Department of General Zoology and Neurobiology, University of Pécs, H-7624 Pécs, Hungary.

(Heidelberger et al., 1994; Schneggenburger and Neher, 2000; Bollmann et al., 2000; Beutner et al., 2001). When similar approaches were used to study hormone release from nonneuronal secretory cells, the relationship between local Ca^{2+} and exocytosis was consistent with only a second- or third-order function (Augustine and Neher, 1992; Heinemann et al., 1994; Voets, 2000), suggesting that a fourth-order or higher relationship may be a unique feature of neuronal exocytosis.

At the first synapse in the visual pathway, signal transfer from the rod photoreceptor to postsynaptic horizontal and bipolar cells exhibits a marked linearity, allowing the waveforms evoked by scotopic light flashes applied to a dark-adapted rod to be accurately reproduced in the postsynaptic neurons (Tranchina et al., 1981; Wu, 1985; Sakai and Naka, 1987; Naka et al., 1987). The source of this unusual synaptic linearity is not known, but one possibility is that the relationship between Ca^{2+} entry and exocytosis in rod photoreceptor terminals is linear (Witkovsky et al., 1997; Thoreson et al., 2003; Armstrong-Gold and Rieke, 2003). The relationship between Ca^{2+} entry and release can be linearized by a sparsely distributed array of Ca^{2+} channels and release sites (reviewed in Augustine et al., 1991) or by the local saturation of Ca^{2+} buffers in the presence of an intracellular diffusion barrier (Kits et al., 1999). In addition, the Ca^{2+} sensor utilized for triggering exocytosis can shape the exocytotic response (see Augustine, 2001), and recent studies have indicated that the isoform of the putative Ca^{2+} sensor for neuronal exocytosis, synaptotagmin, that is enriched in the rod terminal may differ from that found at conventional synapses (Heidelberger et al., 2003; Berntson and Morgans, 2003; Ullrich and Sudhof, 1994; Butz et al., 1999; but see Kreft et al., 2003).

The rod photoreceptor differs from many central neurons in that the release of neurotransmitter from this nonspiking neuron varies smoothly and continuously with changes in membrane potential. In darkness, the resting potential of a rod is typically about −40 mV, which is sufficiently positive to activate Ca^{2+} entry through presynaptic L-type Ca^{2+} channels (Corey et al., 1984) and trigger exocytosis (Schmitz and Witkovsky, 1997). Bright light hyperpolarizes a rod to ~−55 mV, at which potential both Ca^{2+} entry and exocytosis are minimal. In one study, the Ca^{2+} threshold for continuous exocytosis in this neuron was estimated to be in the low micromolar range (Rieke and Schwartz, 1996). By contrast, a 10-fold higher estimate was reported by another group that examined membrane fusion in response to the rapid and global elevation of intracellular Ca^{2+} (Kreft et al., 2003). However, the large pool of membrane that fused in the latter study was poorly defined and greatly exceeded the number of ribbon-associated vesicles (present study; Kreft et al., 2003). Thus, this study may have included contributions from numerous vesicles outside the releasable pool that were not fully prepared for fusion, precluding an accurate comparison of the exocytotic properties of vesicles in the releasable pool between the photoreceptor and other neurons.

In the present study, we examine the fundamental properties of synaptic exocytosis in the rod photoreceptor, making it only the fourth vertebrate neuron to be examined at this level of detail. Our data reveal an unusual linear relationship between Ca^{2+} influx and synaptic exocytosis, and we show that this linearity is at least partly due to the presence of a novel, highly Ca^{2+}-sensitive pool of releasable vesicles. We report that the relationship between the rate of exocytosis and $[Ca^{2+}]_i$ in this central neuron is relatively shallow when compared with the other neurons and, in fact, is nearly linear within a restricted range of intraterminal Ca^{2+}. In the process of achieving these results, we also established the reliability of capacitance measurement as a tool to monitor exocytosis in the rod photoreceptor, and we defined the releasable pool of synaptic vesicles, detailed its fusion kinetics, and described its ultrastructural correlate. Together, our results demonstrate that at the first synapse in the rod visual pathway, the relationship between Ca^{2+} and exocytosis differs from that of the other

characterized neurons, suggesting that in neurons there is a spectrum of Ca^{2+}-dependent presynaptic mechanisms that modulate synaptic transmission.

Results

Exocytosis Evoked by Membrane Depolarization

In the rod photoreceptor, the exocytotic response evoked by Ca^{2+} influx through voltage-gated channels has not been characterized. We used capacitance measurements (Lindau and Neher, 1988) to monitor exocytosis evoked by Ca^{2+} influx in isolated rod photoreceptors that lacked outer segments but retained their synaptic terminals, as illustrated in Figure 1. In this example, a 5 s voltage step from −65 mV to −5 mV triggered a 220 fF increase in capacitance that was followed shortly thereafter by restoration to near its prestimulus value (Figure 1A). No significant changes in the conductance traces G_m and G_s accompanied the stimulus (Figure 1B), indicating that measurements of input resistance and capacitance were adequately separated. In some cells, Ca^{2+} influx did evoke an increase in membrane conductance, but this conductance change did not correlate with the capacitance jump and can be attributed to incomplete blockade of Ca^{2+}-dependent channels (Bader et al., 1982). Consistent with Ca^{2+}-dependent fusion of synaptic vesicles with the plasma membrane, depolarization-triggered capacitance increases were observed only in freshly dissociated photoreceptors with intact synaptic terminals and were blocked by 100 μM external Cd^{2+} (500 ms, −65 to −5 mV, p = 0.0001, unpaired t test, df = 55).

Kinetics of Exocytosis Triggered by Membrane Depolarization

To characterize vesicle pools participating in release from rods, we examined the magnitude of exocytosis evoked by fixed amplitude depolarizations of varying durations (von Gersdorff and Matthews, 1994a; Parsons et al., 1994). In the example shown in Figure 2A (open circles), a 500 ms voltage step evoked a 290 fF increase in membrane capacitance. A 2 s depolarizing step applied later in this same neuron evoked a 480 fF increase (Figure 2A, filled circles). Results from many similar experiments, summarized in Figure 2B, show the increase in capacitance evoked by a depolarizing pulse as a function of pulse duration. This relationship was fit by a dual exponential, indicative of two kinetic components of exocytosis with mean time constants of 5.6 and 298 ms (Figure 2B, solid line). The amplitudes of these components were 92 fF for the faster (inset, Figure 2B) and 210 fF for the slower. Assuming a 45 nm diameter vesicle (see below), this corresponds to the fusion of ~1610 and 3680 vesicles, respectively. The amplitude estimate of the faster component is regarded as an upper limit, since the shortest duration tested (12 ms) was longer than the time constant of the shortest component. The kinetic profile suggests that depolarization of the rod evokes an initial transient burst of release that is followed by a slower rate of release.

Exocytosis was also tested by recording postsynaptic currents (PSC) in OFF bipolar or horizontal cells evoked by depolarizing pulses (−70 to −10 mV) applied to simultaneously recorded presynaptic rods. Glutamate receptor desensitization was inhibited by adding cyclothiazide (0.1 mM) to the bath. In the OFF bipolar cell recording shown in Figure 3A, a short depolarizing pulse of 10 ms applied to the presynaptic rod evoked an inward PSC of 60 pA in the bipolar cell, while a longer depolarizing step of 1 s produced a larger amplitude PSC (150 pA). The initial large PSC declined after 200 ms to a small, sustained current for the remainder of the 1 s pulse. This was typical of the six pairs of cells tested. Since the transient component was observed in the presence of cyclothiazide and in ON bipolar cells (Armstrong-Gold and Rieke, 2003; W.B.T., unpublished), which utilize mGluR6 receptors (Thoreson and Witkovsky, 1999), this component is unlikely to reflect glutamate receptor desensitization. It may instead reflect an initial burst of exocytosis that subsides within a couple hundred ms to a slower sustained rate of release.

To establish the validity of capacitance measurements as a measure of exocytosis in rods, the magnitude of the secretory responses obtained from capacitance measurements and paired recordings were compared. As an index of cumulative vesicle fusion, PSC charge transfer in OFF bipolar and horizontal cells was integrated over time. The magnitude of the capacitance increase was plotted against PSC charge transfer evoked by depolarizing steps of identical duration (Figure 3B). The two measures of exocytosis were linearly correlated ($r^2 = 0.92$), demonstrating that capacitance measurements provide an accurate measure of exocytosis under these conditions. Similar results were seen when the glutamate uptake inhibitor TBOA (0.1 mM) and CPPG (0.3 mM), a metabotropic glutamate receptor antagonist, were also included in the bath during paired recordings ($n = 5$; $r^2 = 0.96$).

The Magnitude of Exocytosis Tracks I_{Ca}

The voltage dependence of the exocytotic response in rod photoreceptors (Figure 4, circles, left axis) closely matched the current-voltage relationship for rod photoreceptor I_{Ca} (Figure 4, data trace, right axis). Capacitance increases were evoked by 100 ms voltage steps from a holding potential of −65 mV to various test potentials; I_{Ca} was measured using a ramp voltage protocol (0.5 mV/ms from −90 to +60 mV). Linear regression of the relationship between I_{Ca} and the depolarization-evoked capacitance jump showed a strong correlation ($r^2 = 0.98$). The linear relationship between I_{Ca} and exocytosis at this synapse (Figure 4) contrasts markedly with observations at other CNS synapses, including the retinal bipolar cell, which typically show a third or fourth power relationship between I_{Ca} and exocytosis (Mintz et al., 1995; Borst and Sakmann, 1999; Wu et al., 1999; von Gersdorff and Matthews, 1994a).

Rods Contain a Highly Ca^{2+}-Sensitive Pool of Vesicles

To explore the basis of the linear relationship between I_{Ca} and exocytosis, we probed the Ca^{2+} dependence of the release machinery. Exocytosis was triggered by flash photolysis of Ca^{2+}-loaded DM-nitrophen. The rapid and spatially homogenous increase in Ca^{2+} provided by flash photolysis allows the spatially averaged intraterminal $[Ca^{2+}]$ to be used as an index of the local Ca^{2+} concentration near release sites (Heidelberger et al., 1994; Schneggenburger and Neher, 2000; Beutner et al., 2001).

The concentration of Ca^{2+} required to trigger exocytosis in rods was much lower than that needed to evoke phasic release from bipolar cells (Heidelberger et al., 1994; Heidelberger, 1998). For example, an abrupt increase in rod intraterminal $[Ca^{2+}]$ to 780 nM (Figure 5A) triggered a slowly developing 85 fF increase in membrane capacitance (Figure 5B). There were no correlated changes in the conductance traces G_m and G_s (Figures 5C and 5D). After exhausting the releasable pool of vesicles, flash photolysis evoked similar conductance changes without accompanying capacitance jumps. Flashes applied to rods dialyzed with unloaded DM-nitrophen (5 mM DM-nitrophen, 0 mM Ca^{2+}) did not trigger capacitance increases ($n = 6$). Thus, photolytic release of Ca^{2+} triggered a true increase in membrane capacitance. As in other neurons, endocytosis was not observed during the 2 s following the flash, presumably due to experimental conditions (0 ATP and high, post-flash Ca^{2+}; Heidelberger, 2001a; von Gersdorff and Matthews, 1994b; Rouze and Schwartz, 1998) and a lag between exocytosis and endocytosis (Rieke and Schwartz, 1996).

To determine the rate of exocytosis, the rising phase of the capacitance increase triggered by flash photolysis of caged Ca^{2+} in each rod was fit with a single exponential function. For the response depicted in Figure 5B, the time constant of this single exponential fit was 588 ms. The rate constants ($1/\tau$) describing the capacitance rises of 45 rod photoreceptors are plotted in Figure 6 as a function of intraterminal $[Ca^{2+}]$ measured immediately after the flash. The

figure shows that the rate of membrane addition was dependent upon the magnitude of the Ca^{2+} rise and that exocytosis was reliably triggered by submicromolar Ca^{2+}.

Our knowledge of intraterminal Ca^{2+} levels in rods is limited, but Rieke and Schwartz (1996) estimated that spatially averaged, intraterminal Ca^{2+} ranges from 0.5 to 3 μM in light and dark. Similarly, they showed that global elevation of $[Ca^{2+}]$ from 0.4 to 2 μM produced substantial exocytosis, whereas global reduction below 0.7 μM significantly decreased exocytosis (Rieke and Schwartz, 1996). Our results show that between 0.5 and 3 μM $[Ca^{2+}]$, the rate of exocytosis in rod terminals increased in a nearly linear fashion with $[Ca^{2+}]$, as illustrated by the linear regression (solid line) fit to data points within this range (black circles). The shallow slope of the rate versus $[Ca^{2+}]_i$ relationship combined with a restricted $[Ca^{2+}]_i$ range can thus contribute to the linearity between I_{Ca} and exocytosis.

The Same Vesicles Participate in Both Flash- and Depolarization-Evoked Release

To test whether the pool of vesicles that exocytose in response to flash photolysis of caged Ca^{2+} also fuse in response to influx through voltage-gated Ca^{2+} channels, we performed cross depletion experiments. Using a protocol similar to Heidelberger (1998), a 2 s depolarization was given to trigger exocytosis of vesicles capable of fusion in response to Ca^{2+} influx through voltage-gated Ca^{2+} channels and deplete the releasable pool (Figure 7). This was followed by a maximal UV flash to liberate Ca^{2+} from DM-nitrophen and trigger the fusion of vesicles in the highly Ca^{2+}-sensitive pool. The mean amplitude of flash-evoked capacitance jumps following a depolarizing voltage step was significantly smaller ($p = 0.03$) than the mean capacitance increase evoked by flashes that were not preceded by a voltage step. The residual flash-evoked capacitance increase evoked in cells following prior depolarization may reflect pool refilling during the interval (≤10 s) between the voltage step and the flash, consistent with the time constants of refilling (<8 s) reported for several different neurons (reviewed in Heidelberger, 2001b). It may also reflect an inability to fully deplete the pool of available vesicles with steps of up to 2 s (Beutner et al., 2001). However, there is clearly substantial overlap between the highly Ca^{2+}-sensitive pool of vesicles released by flash photolysis and the pool of synaptic vesicles released by the physiological stimulus for glutamate release, Ca^{2+} entry.

Ultrastructural Analysis of Rod Active Zones

To estimate the number of vesicles tethered to presynaptic ribbons, we analyzed electron micrographs of rod terminals. Ribbons in isolated cells look identical to those in vivo (Figure 8). The surface area of the average ribbon was measured using electron micrographs that were previously prepared for serial reconstruction (see Townes-Anderson et al., 1985). Because photoreceptor ribbons tend to be rectangular in shape (see Pierantoni and McCann, 1981; Townes-Anderson et al., 1985), the maximum length of a ribbon in a single thin section was multiplied by the number of sections in which the ribbon appeared, assuming a section width of 80 nm for each section. The surface area of the ribbon face averaged 0.97 ± 0.19 μm^2 (15 ribbons; two terminals), in agreement with estimates obtained from the serial reconstruction of two rod ribbons ($ribbon_1 = 0.98\ \mu m^2$; $ribbon_2 = 1.2\ \mu m^2$). These values are also similar to surface area measurements of 1.05 μm^2 for cone pedicles in the frog retina, which are morphologically similar to salamander rods (Pierantoni and McCann, 1981). Salamander rods average 7.3 ribbons/synaptic terminal, but only 5 remain attached to the plasma membrane following dissociation and are presumed to be functional (Townes-Anderson et al., 1985). The total surface area of functional ribbons/terminal in an isolated rod is therefore estimated to be 9.72 μm^2. Lining the ribbon along each dimension is an average of 17.65 ± 0.79 vesicles/μm (17 ribbons; 6 terminals; 5 animals). We extended this to two dimensions by assuming a hexagonal array (e.g., see Figure 8B, arrowheads; Pierantoni and McCann, 1981) to yield 339.6 vesicles/μm^2 or 3301 vesicles for 5 ribbons.

Approximately 250 more vesicles line the ribbon edges, suggesting there are ~3550 ribbon-associated vesicles/rod terminal or ~710 vesicles/ribbon.

Maximal vesicle diameters were found to range from an average of 42.2 nm in fixed cells (30 vesicles; 3 terminals; 3 animals) to 46 nm in rapidly frozen cells (20 vesicles; 2 terminals; 1 animal). Because of potential differences in size between maturing synaptic vesicles and those ready for release, diameters were measured only for vesicles attached to ribbons. It is assumed that rapidly frozen tissue displays ultrastructure closer to its native state because cellular activity is stopped within milliseconds, before significant osmotic effects can distort morphology (Tatsuoka and Reese, 1989). Assuming, therefore, a vesicle diameter of 45 nm and a specific membrane capacitance of 0.9 $\mu F/cm^2$ (Gentet et al., 2000), the capacitance per vesicle is 57 aF, similar to the value of 65 aF/vesicle obtained by directly measuring the capacitance change produced by a single fusion event in the calyx of Held (Sun et al., 2002).

Using 57 aF/vesicle, the average amplitude of the exocytotic response in flash experiments (171 fF) corresponds to the fusion of 3000 vesicles. This may represent a lower limit for the number of vesicles in the releasable pool since some vesicles may fuse during the brief Ca^{2+} spike that occurs after achieving the whole-cell configuration, when cytosolic Mg^{2+} replaces some of the Ca^{2+} bound to DM-nitrophen (Neher and Zucker, 1993; Parsons et al., 1994); these vesicles may not be functionally replaced in the absence of MgATP (Heidelberger, 2001b; Heidelberger et al., 2002). The 5350 vesicles (305 fF) released by a 2 s depolarizing step provides an upper limit for vesicles in the releasable pool because some pool refilling is likely to occur during a 2 s depolarization and some vesicles away from the ribbons may undergo fusion as submembrane $[Ca^{2+}]$ builds. Thus, physiological estimates of the releasable vesicles bracket the morphological estimate of ~3550 vesicles bound to ribbon-style active zones.

Discussion

The present study characterizes the voltage dependence, Ca^{2+} dependence, release kinetics, and ultrastructural correlates of synaptic transmission at the rod photoreceptor ribbon synapse. Only three other neurons have been studied at this level of detail. Although the rod photoreceptor shares some presynaptic behavior with these other neurons, it also exhibits unique features that expand the dynamic range of Ca^{2+}-dependent neurotransmitter release and permit it to relay information about graded changes in light intensity.

Like several sensory neurons, the rod photoreceptor has ribbon-style active zones (e.g., see Figure 8), but the role of the ribbon in synaptic transmission remains in question (Lenzi and von Gersdorff, 2001; Parsons and Sterling, 2003). In the bipolar cell, there is good agreement between the number of vesicles released by brief depolarizations and the number of vesicles tethered to ribbons, suggesting that the ribbon tethers vesicles that are primed for release (von Gersdorff et al., 1996). Likewise, in the present study, we found that the total number of tethered vesicles estimated from our ultrastructural analysis of rod ribbon-style active zones (3550 vesicles/terminal) lies within the bounds established by our physiological assays of pool size (3000–5350 vesicles). In addition, our paired pre- and postsynaptic recordings revealed a pronounced initial transient component to the depolarization-evoked EPSC in second-order retinal neurons that subsided within 200 ms, even after blocking glutamate receptor desensitization (Figure 3). We hypothesize that this initial, large burst of exocytosis reflects the release of synaptic vesicles tethered to the ribbons since a 200 ms depolarization stimulates release of 3500 vesicles, nearly the same number of vesicles as found in the releasable pool.

Pulse duration experiments uncovered two kinetic components of release (Figure 2). The estimated time constant of the faster component was 5.6 ms, which is less than the shortest test step of 12 ms and thus subject to some error. A similarly fast time constant was reported in bipolar cells (1.6 ms; Mennerick and Matthews, 1996) and hair cells (10 ms; Moser and Beutner, 2000). This fast component may arise from the fusion of vesicles in a rapidly releasable pool. As in the bipolar cell (Mennerick and Matthews, 1996), the rate of exocytosis in rods may be limited by the kinetics of I_{Ca}, which activates with time constants of 1–5 ms (Corey et al., 1984). The slower component of release in rods exhibited a time constant comparable to the slower component of the bipolar cell that characterizes the entire releasable pool (Mennerick and Matthews, 1996; Heidelberger, 2001b). This slow component is unlikely to reflect the kinetics of inactivation of rod I_{Ca} because the latter exhibits a much slower time constant of ~1.7 s (Rabl and Thoreson, 2002).

Chow et al. (1994) assumed that similar Ca^{2+} increases evoked by membrane depolarization or flash photolysis of caged Ca^{2+} would stimulate similar rates of exocytosis. By comparing the rates of exocytosis achieved in pulse duration experiments with rates achieved following flash photolysis of caged Ca^{2+}, they thus estimated the average [Ca^{2+}] experienced by the release machinery of chromaffin cells (Chow et al., 1994). Using this same approach, we estimate that fusion of the average vesicle represented by the larger, slower kinetic component of release (τ = 298 ms) is likely to experience ~1 μM Ca^{2+}. By contrast, the slower kinetic component of exocytosis in bipolar cells probably experiences 20–50 μM Ca^{2+} (Heidelberger, 2001b). The present data does not allow us to directly estimate the predicted Ca^{2+} concentration experienced by the faster component of release (τ = 5.6 ms). However, an extension of the linear fit that describes the relationship between the rate of exocytosis and Ca^{2+} (Figure 6) suggests that to achieve a rate of 179 s^{-1} ($1/\tau$), the Ca^{2+} concentration need not exceed ~30 μM, assuming that the same Ca^{2+} sensor was used to release this component. Similarly, if we use the three Ca^{2+} binding site model (discussed below and in Experimental Procedures), we find that Ca^{2+} need not exceed 45 μM and could be as low as 20 μM, depending upon model parameters. By contrast, the fastest component of exocytosis in the bipolar cell most likely experiences ~325 μM $[Ca^{2+}]_i$ (Mennerick and Matthews, 1996; Heidelberger, 2001b). The high Ca^{2+} sensitivity suggested for the major kinetic component of release in the present study indicates that in the rod, a vesicle in the releasable pool does not have to experience the high [Ca^{2+}] thought to exist near the mouth of an open Ca^{2+} channel in order to undergo fusion. Vesicles in the smaller, rapidly releasable pool in the rod also appear more sensitive to Ca^{2+} than those of other neurons.

An extension of this hypothesis is that exocytosis in rods is regulated by changes in the spatially averaged levels of intraterminal [Ca^{2+}] rather than the high [Ca^{2+}] found in microdomains immediately surrounding individual Ca^{2+} channels (Rieke and Schwartz, 1996). Consistent with this possibility, we found that exocytosis in rods operated at submicromolar [Ca^{2+}] (Figure 6), confirming an earlier estimate (Rieke and Schwartz, 1996). This contrasts substantially with the 8–10 μM Ca^{2+} threshold for exocytosis determined for bipolar cells and hair cells using almost identical experimental approaches (Heidelberger et al., 1994; Heidelberger, 1998; Beutner et al., 2001). Bipolar cells may also possess a low threshold component of exocytosis (Lagnado et al., 1996; Rouze and Schwartz, 1998); however, this component is difficult to detect with electrophysiological techniques (von Gersdorff and Matthews, 1994a; Heidelberger et al., 1994; von Gersdorff et al., 1998), indicating that it may represent a minor component of release. By contrast, the amplitude of the low threshold pool in the rod is large and similar in size to the number of ribbon-associated vesicles. A recent report raises the possibility that a second component of membrane addition with a high-threshold Ca^{2+} sensor may co-exist with the low-threshold pool in the rod photoreceptor (Kreft et al., 2003). However, in contrast to the pool studied here, the functional significance of the high-threshold pool is difficult to interpret, as it has

not been associated with neurotransmitter release or shown to be cross-depleted by a physiological stimulus. Nonetheless, it is conceivable that, as has been suggested for bipolar cells (Lagnado et al., 1996) and for hippocampal neurons (Geppert et al., 1994), two different Ca^{2+} sensors for exocytosis may co-exist in the rod.

The relationship between the rate of fusion of vesicles in the releasable pool and intraterminal [Ca^{2+}] in the rod is not as steep as expected for a neuron. For a one log unit change in intraterminal Ca^{2+}, the rate of exocytosis in the rod photoreceptor changed by less than one log unit (Figure 6), whereas a one log unit increase in Ca^{2+} produced an approximately two log unit increase in rate in bipolar cells and hair cells (Heidelberger et al., 1994; Beutner et al., 2001). Furthermore, in the other characterized neurons, the Ca^{2+} dependence of the rate of exocytosis is described by a mathematical model that assumes that membrane fusion is triggered by the sequential binding of at least four Ca^{2+} ions to unidentified Ca^{2+} binding sites (Heidelberger et al., 1994; Beutner et al., 2001; Schneggenburger and Neher, 2000). By contrast, a model incorporating four independent Ca^{2+} binding steps that precede the final fusion step does not adequately describe the rod data (see Experimental Procedures for a description of the modeling). Rather, the relatively shallow relationship between rate of exocytosis and [Ca^{2+}] is reminiscent of a neuroendocrine cell (Augustine and Neher, 1992; Heinemann et al., 1994; Voets, 2000). Indeed, the releasable pool in the rod closely resembles the highly Ca^{2+}-sensitive pool of secretory vesicles in chromaffin cells (Yang et al., 2002), and like the chromaffin cell, the rod data can be modeled assuming no more than three Ca^{2+} binding steps (Figure 6, dotted line). However, more experiments are needed to precisely define the free parameters of the rod model and distinguish between one, two, and three binding sites.

Under conditions thought to mimic physiological Ca^{2+} levels experienced by rods in light and dark (~0.5–3 μM $[Ca^{2+}]_i$; Rieke and Schwartz, 1996), the relationship between the rate of exocytosis and $[Ca^{2+}]_i$ was nearly linear (Figure 6). These results are consistent with the finding of a linear correlation between the time course of slow, global elevations in $[Ca^{2+}]_i$ and the accompanying increases in membrane capacitance (Rieke and Schwartz, 1996). The linear relationship between the rate of exocytosis and $[Ca^{2+}]_i$ in this restricted range very likely contributes to the unusual linearity that we found between the magnitude of exocytosis and I_{Ca} (Figure 4), which in turn contributes to linearity in the transmission of signals from rod photoreceptors to their postsynaptic targets (Tranchina et al., 1981; Sakai and Naka, 1987; Naka et al., 1987; Wu, 1985). As suggested by Figure 4, a rod can translate a small light-evoked hyperpolarization from the dark potential into a small change in the magnitude of I_{Ca} and exocytosis. With larger light-evoked voltage excursions, the sigmoidal relationship between I_{Ca} and rod membrane potential will become increasingly evident, consistent with the observation that with large changes in illumination, there is a decrease in gain of the synaptic transfer from a rod to its second-order neurons (Attwell et al., 1987; Wu, 1988; Belgum and Copenhagen, 1988; Witkovsky et al., 1997).

Other mechanisms, in addition to a shallow relationship between the rate of release and $[Ca^{2+}]_i$, may contribute to the observed linearity between I_{Ca} and exocytosis. For example, if the microdomains of Ca^{2+} that surround individual release sites do not overlap, the number of active release sites could increase linearly with the number of open Ca^{2+} channels, obscuring any cooperativity between Ca^{2+} and release that may exist at any one release site (Augustine et al., 1991). However, the low Ca^{2+} threshold of release suggests that spatially averaged Ca^{2+} levels can regulate release and argues against the presence of nonoverlapping Ca^{2+} microdomains in the rod terminal.

An alternative scenario involving local buffer saturation and the presence of an intracellular diffusion barrier has been proposed to account for linearization of the power law relationship

between Ca^{2+} and exocytosis in neuroendocrine cells (Kits et al., 1999). Such a mechanism might also contribute to linearizing the relationship between exocytosis and influx through the L-type Ca^{2+} channels localized to ribbon-style active zones in the rod terminal (Nachman-Clewner et al., 1999; Morgans, 2001; Berntson et al., 2003). Freeze fracture studies of rod terminals reveal an aggregation of particles concentrated on the synaptic ridge below the arciform density that are "polyhedral in shape and often contain a minute central dimple" (Raviola and Gilula, 1975) and are similar in size to particles tentatively identified as L-type Ca^{2+} channels in freeze fracture electron micrographs of hair cell synapses (Roberts et al., 1990). If Ca^{2+} channels are clustered at the apex of the synaptic ridge, then the adjacent arciform density might act as a local diffusion barrier that allows Ca^{2+} to spill over onto the ribbon face only after saturating local buffers. This would minimize the contribution of microdomains and also contribute to linearity between I_{Ca} and release (Kits et al., 1999).

The present study demonstrates that a high Ca^{2+} affinity mechanism governs exocytosis from rods, extending the results of Rieke and Schwartz (1996). In contrast, bipolar cells have a prominent exocytotic response that is dominated by a low-affinity Ca^{2+} sensor. This difference may support different response characteristics in these two neurons. The ON bipolar cell responds to light with a transient depolarization that drives spiking neurons, whereas the graded, hyperpolarizing light responses in the rod drives graded responses in second-order neurons. Consider too that rods release glutamate continuously in the dark. With time, the L-type Ca^{2+} channels responsible for triggering exocytosis (Schmitz and Witkovsky, 1997) will undergo Ca^{2+}-dependent inactivation (Corey et al., 1984; Rabl and Thoreson, 2002). If the Ca^{2+} sensor were a high-threshold, low-affinity Ca^{2+} sensor, then inactivation of a given channel could result in the failure of its nearby vesicle(s) to fuse. This failure of fusion would erroneously signal an increase in illumination. However, if the Ca^{2+} sensors are tuned to spatially averaged $[Ca^{2+}]_i$, then the activity of any one Ca^{2+} channel is less critical to the overall magnitude of release. A high-affinity receptor may also minimize the need for large Ca^{2+} loads that might otherwise be achieved during periods of prolonged darkness, reducing the potential for photoreceptor damage.

Experimental Procedures

Photoreceptor Isolation and Slice Preparation

Aquatic tiger salamanders (*Ambystoma tigrinum*, 18–25 cm) were cared for according to institutional guidelines. For both isolated cell and slice preparations, an eye was enucleated after rapid decapitation, the anterior section was removed, and the eyecup was cut into quarters.

Isolated rods were prepared by enzymatic digestion followed by mechanical trituration using previously published protocols (Rabl and Thoreson, 2002). Cells were plated on slides coated with a salamander-specific antibody, Sal-1 (courtesy of P. MacLeish, Morehouse School of Medicine), or concanavalin A (1 mg/ml). Recordings were begun after letting cells attach for 10–15 min. Recording medium contained (in mM): 106 NaCl, 2.5 KCl, 1.8 $CaCl_2$, 0.5 $MgCl_2$, 5 CsCl, 10 HEPES, and 5 or 11 glucose (pH 7.8). In some cases, 0.1 mM niflumic acid was added to block $I_{Cl(Ca)}$. To minimize noise in the capacitance records, only photoreceptors whose outer segments were lost during the dissociation process were studied. Unless otherwise noted, all rods had a visible synaptic terminal.

Retinal slices were prepared as described elsewhere (Rabl and Thoreson, 2002). For PSC recordings, slices were superfused with a solution containing (in mM): 111 NaCl, 2.5 KCl, 1.8 $CaCl_2$, 0.5 $MgCl_2$, 10 HEPES, and 5 glucose. For recordings of I_{Ca}, the superfusate contained (in mM): 95 NaCl, 2.5 KCl, 2 $CaCl_2$, 0.5 $MgCl_2$, 5 CsCl, 10 TEA

(tetraethylammonium) Cl, 10 HEPES, 5 glucose, 0.1 niflumic acid. Unless otherwise specified, chemicals were obtained from Sigma/RBI (St. Louis, MO).

Electrical Recordings

Conventional whole-cell voltage-clamp recordings were made using 5–12 MΩ patch pipettes pulled from borosilicate and coated with Sylgard (Dow Corning, Midland, MI) to reduce stray capacitance. The pipette solution for voltage-step experiments during capacitance recordings contained (in mM): 94 CsGluconate, 9.4 TEACl, 1.9 mM $MgCl_2$, 9.4 mM MgATP, 0.5 mM GTP, 0.5 mM EGTA, 32.9 mM HEPES (pH 7.2). For paired recordings from pre- and postsynaptic neurons, the perforated patch method with gramicidin was used (Kyrozis and Reichling, 1995). For these recordings, the pipette solution contained (in mM): 54 CsCl, 61.5 $CsCH_3SO_3$, 3.5 NaCl, 10 HEPES (pH 7.2). Gramicidin stocks were made with ethanol (5 mg/ml) and used at a final concentration of 5 μg/ml.

The intracellular solution for flash photolysis experiments was designed to produce a step-like change in intraterminal Ca^{2+} (Heidelberger et al., 1994; Heinemann et al., 1994; Heidelberger, 1998). It contained (in mM): 72 Cs Gluconate, 6 mM TEACl, 2.5 mM NaCl, 5 mM DM-nitrophen (Molecular Probes, Eugene, OR), 5 mM $CaCl_2$, 2 mM DPTA, 1 mM Fura-FF (Molecular Probes), and 55 Cs HEPES. To avoid complications related to the possibility of an undetected Ca^{2+} spike that might be caused by the rebinding of Ca^{2+} to unphotolyzed and unloaded DM-nitrophen after a flash, we experimentally determined the concentration of our nominally 100 mM DM-nitrophen stock solution by titrating against Ca^{2+} standards. For each DM-nitrophen internal solution, an aliquot was removed prior to the addition of Fura-FF and the free Ca^{2+} measured with Fura-2 (Molecular Probes). Solutions were discarded if free $Ca^{2+} > 350$ nM. Calculations indicate that DM-nitrophen was 99% loaded under these conditions. In most instances, electrical recordings were made from the cell body although a few recordings were made from the axon terminal. Charging curves of isolated rods were fit by similar single exponentials regardless of whether the pipette was placed on the cell body or terminal, indicating that rods form a single electrotonic compartment (see Supplemental Data at http://www.neuron.org/cgi/content/full/42/4/595/DC1).

Voltage ramps (0.5 mV/ms) from −90 to +60 mV were used to measure I_{Ca}. The ohmic leak conductance was subtracted. A junction potential of −9.3 mV calculated using PClamp software (Axon Instruments, Foster City, CA) was subtracted.

Capacitance Measurements

Capacitance measurements in isolated rods were typically made using a dual sine wave voltage stimulus protocol (Rohlicek and Schmid, 1994; Donnelly, 1994; see also Gillis, 1995). Cells were held at −70 or −65 mV, and a dual sine wave voltage stimulus (15 mV peak) of 390.6 and 781.2 Hz was applied about the DC holding potential. This was implemented using JClamp software (SciSoft, New Haven, CT), Digidata 1322 interface (Axon Instruments), and Axopatch 200B amplifier (Axon Instruments). Admittance analysis was performed on the Fast Fourier Transform (FFT) of the current response every 2.56 ms, yielding estimates of membrane capacitance (C_m), series resistance (R_s), membrane resistance (R_m), and DC current. In some experiments, a computer-controlled EPC-9 patch clamp amplifier (HEKA Elektronik, Lambrecht, Germany) equipped with EPC-9 Pulse software (HEKA Elektronik) was used to apply an 800 Hz, 15 mV peak voltage stimulus about the DC holding potential. This stimulus was similar to that used previously to study exocytosis in rods (Rieke and Schwartz, 1996). The resulting current was then analyzed using the software emulation of a two-phase lock-in amplifier provided by Pulse to obtain estimates of C_m, R_s, and R_m following the method of Lindau and Neher (1988). In high-

resolution mode, one capacitance data point was generated and collected per sine wave cycle. In time-resolved mode, one data point was generated per 100 ms sine wave segment. With both capacitance measurement techniques, the membrane potential remained below the activation range of the voltage-gated Ca^{2+} channels (Figure 2; Rieke and Schwartz, 1996), and both approaches yielded similar results.

Recordings of Postsynaptic Currents

For paired recordings, rods and adjacent postsynaptic neurons were simultaneously voltage clamped using a Multiclamp amplifier (Axon Instruments). Currents were acquired and analyzed using Clampex 8.0 software (Axon Instruments).

Rods were voltage clamped at −70 mV, bipolar cells at −50 mV, and horizontal cells at −40 mV. Rods were identified by their characteristic outer segments. Horizontal and OFF bipolar cells exhibited inward currents evoked by depolarizing steps applied to presynaptic rods. PSCs in both cell types are mediated by non-NMDA ionotropic glutamate receptors (Kim and Miller, 1991, 1993) and were studied in the presence of cyclothiazide (0.1 mM) to inhibit glutamate receptor desensitization. Charging curves for bipolar cells were fit by a single exponential, indicating a compact electrotonic structure (<0.1 λ).

Fluorescence Measurements and Flash Photolysis of Caged Ca^{2+}

Fluorescence measurements of $[Ca^{2+}]_i$ were obtained from the terminals of isolated rods. Fura-FF was alternately excited at 340 or 380 nm and emitted fluorescence monitored at 510 nm. Digital fluorescent images were obtained with a cooled CCD camera (Sensi-Cam, Cooke Corp., La Jolla, CA) on an upright fixed stage microscope (Nikon E600FN, Garden City, NY) equipped with a 60× (1.0 N.A.) water immersion objective. Axon Imaging Workbench (AIW 2.2, Axon Instruments) was used to control the camera, filter wheel (Lambda 10-2, Sutter Instruments, Novato, CA), and image acquisition. Pixel binning (8 × 8) of the images was used to decrease acquisition time to 300 ms/image pair. In some experiments, a computer-controlled monochrometer controlled the wavelength of fluorescence excitation (ASI/T.I.L.L. Photonics, Gräfeling, Germany; Messler et al., 1996). In these instances, emitted fluorescence was collected from a rod terminal by means of an adjustable aperture that excluded light from other regions of the object plane. The signal was detected with a photomultiplier tube (R928; Hamamatsu Phototonics, Bridgewater, NJ), sampled by the EPC-9, and acquired with the Fura extension of the Pulse software (HEKA Elektronik).

DM-nitrophen was photolyzed by flashes of UV light derived from a Xenon arc flash lamp (Rapp Optoelectronic, Hamburg, Germany) centered on the rod terminal and coupled through the epifluorescence port of the microscope (Zeiss Axiovert 100, Thornwood, NY; or Nikon E600FN). Photolysis of DM-nitrophen allows rapid and uniform increases in $[Ca^{2+}]_i$ throughout the terminal (Naraghi et al., 1998). Flash intensity was varied to adjust the amount of photolysis and thus the magnitude of intraterminal Ca^{2+} elevation (e.g., Heidelberger et al., 1994).

Intraterminal Ca^{2+} was calculated from the ratio of emitted light at 340 nm and 380 nm (Grynkiewicz et al., 1985) using calibration constants determined in cells with established methods. Because nerve terminals can actively and rapidly extrude Ca^{2+} (Zenisek and Matthews, 2000; Morgans et al., 1998; Helmchen et al., 1997), calibrations were performed on cell somas using intracellular solutions that lacked ATP. For voltage-step experiments, calibration constants were determined by dialyzing cells with highly buffered, known concentrations of Ca^{2+} (e.g., Heidelberger and Matthews, 1992). For flash photolysis experiments, the calibration constants were obtained in three different ways, each of which

yielded an estimate of the Ca^{2+} threshold for exocytosis similar to that reported by Rieke and Schwartz (1996). The first approach was adapted from Heinemann et al. (1994) and takes into account photolysis efficiency and the bleaching of DM-nitrophen and Fura-FF by the UV flash. The second approach used highly buffered internal solutions in which DM-nitrophen served as the exogeneous Ca^{2+} buffer. In the third approach, Keff with Fura-FF was verified by dialyzing isolated retinal neurons with a HEDTA-buffered solution with a free Ca^{2+} concentration of 5.4 μM determined using MaxChelator and confirmed with a Ca^{2+}-sensitive electrode (KwikCal, World Precision Instruments). The calibration solution contained (in mM): 75 CsGluconate, 10 TEACl, 2.5 NaCl, 10 HEDTA, 5 $CaCl_2$, 35 HEPES. A similar Keff was obtained using an EGTA-buffered solution (110 KCl, 3.5 NaCl, 2 glucose, 2 EGTA, 2 $CaCl_2$, 5 HEPES) with a calculated free Ca^{2+} concentration of 18 μM. The minimum and maximum ratios were determined, respectively, by dialyzing retinal neurons with 0 Ca^{2+} plus 5 mM DM-nitrophen (unloaded DM-nitrophen) or 10 mM Ca^{2+} plus 5 mM DM-nitrophen (fully loaded DM-nitrophen) solutions. Under the conditions of this study (low chelator concentration and low flash intensity), correction of the calibration constants for flash-related changes in fluorescence was not required.

Ultrastructural Studies

Data collected for estimates of the number of vesicles tethered to presynaptic ribbons came from electron micrographs of isolated salamander rods previously used for serial reconstruction of rod terminals (Townes-Anderson et al., 1985) or similarly prepared but randomly sectioned. Ribbon surface area can vary with illumination and time of day (Abe and Yamamoto, 1984; Adly et al., 1999). The salamander rod cells used for ultrastructural and physiological experiments were both prepared using similar cell isolation procedures under room lights during daytime. For morphology, cells were fixed 2 hr after plating. Primary fixation was done with a mixture of 2.5% glutaraldehyde, 2.5% paraformaldehyde, and 0.05% picric acid in 0.1 M cacodylate buffer (pH 7.4). Tissue preparation and electron microscopical techniques are described in Townes-Anderson et al. (1985). For analysis of synaptic vesicle diameter, isolated salamander rod cells fixed chemically, as above, or by rapid freezing and freeze-substitution were examined. Techniques for freezing and freeze-substitution followed those described in Townes-Anderson et al. (1988).

Analysis

To determine the rate constant for exocytosis, the rising phase of the capacitance change was fit with a single exponential using either JClamp or IgorPro 4.0 software (Wavemetrics, Inc., Lake Oswego, OR). Postsynaptic currents and rod I_{Ca} were analyzed using PClamp software. The criterion for statistical significance was chosen to be $p < 0.05$ and evaluated with Student's t test using GraphPad Prism 2.0 (San Diego, CA). Variability is reported as ±SEM.

Model simulations of the rate versus Ca^{2+} data (Figure 6, dashed line) were performed in Igor. One kinetic model for the rod, adapted from published models of exocytosis (Heinemann et al., 1994; Heidelberger et al., 1994; Voets 2000; Schneggenburger and Neher 2000), consists of a series of three Ca^{2+} binding steps followed by vesicle fusion:

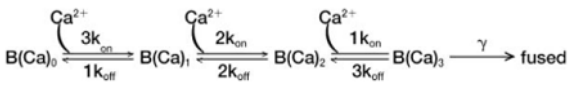

The differential equations describing vesicle fusion kinetics were solved using Igor's IntegrateODE function. The initial pool size, $B(Ca)_0$, was taken from the mean capacitance

response to a flash (171 fF). The final fusion rate constant, γ, was set to 300 s^{-1}, a value slightly larger than the maximum fusion rate observed in pulse-duration experiments as previous work in bipolar cells has shown that the maximal fusion rate in pulse-duration experiments and flash photolysis experiments are similar (Mennerick and Matthews, 1996; Heidelberger, 1998). In addition, γ = 3000 s^{-1}, which is faster than the maximum rate in the bipolar cell (Heidelberger et al., 1994) but slower than the maximum rate in hair cells (Beutner et al., 2001) and γ = 200 s^{-1} were also tested. Changes in γ did not affect the slope of the rate Ca^{2+} relation; however, it did effect the estimated Ca^{2+} concentration experienced by the fast component of release. Forward (k_{on}) and backward (k_{off}) rate constants for the Ca^{2+} binding steps were adjusted to achieve a good correspondence with the data. The simulation shown in Figure 6 was calculated with $k_{on} = 10 \times 10^6$ $M^{-1}s^{-1}$ and $k_{off} = 9$ s^{-1}.

Supplementary Material

Refer to Web version on PubMed Central for supplementary material.

Acknowledgments

This study was supported by NEI grants EY-10542, EY-12128, EY-12031, and EY-10608, Research to Prevent Blindness, Gifford Foundation, Coalition for Brain Injury Research, and the Esther and Joseph Klingenstein Fund. We thank Gary Matthews and Paul Witkovsky for suggestions to the manuscript.

References

Abe H, Yamamoto TY. Diurnal changes in synaptic ribbons of rod cells of the turtle. J Ultrastruct Res. 1984; 86:246–251. [PubMed: 6544862]

Adly MA, Spiwoks-Becker I, Vollrath L. Ultrastructural changes of photoreceptor synaptic ribbons in relation to time of day and illumination. Invest Ophthalmol Vis Sci. 1999; 40:2165–2172. [PubMed: 10476779]

Armstrong-Gold CE, Rieke F. Band-pass filtering at the rod to second-order cell synapse in salamander (*Ambystoma tigrinum*) retina. J Neurosci. 2003; 23:3796–3806. [PubMed: 12736350]

Attwell D, Borges S, Wu SM, Wilson M. Signal clipping by the rod output synapse. Nature. 1987; 328:522–524. [PubMed: 3039370]

Augustine GJ. How does calcium trigger neurotransmitter release? Curr Opin Neurobiol. 2001; 11:320–326. [PubMed: 11399430]

Augustine GJ, Neher E. Calcium requirements for secretion in bovine chromaffin cells. J Physiol. 1992; 450:247–271. [PubMed: 1432709]

Augustine GJ, Charlton MP, Smith SJ. Calcium entry and transmitter release at voltage-clamped nerve terminals of squid. J Physiol. 1985; 367:163–181. [PubMed: 2865362]

Augustine GJ, Adler EM, Charlton MP. The calcium signal for transmitter secretion from presynaptic nerve terminals. Ann N Y Acad Sci. 1991; 635:365–381. [PubMed: 1683754]

Bader CR, Bertrand D, Schwartz EA. Voltage-activated and calcium-activated currents studied in solitary rod inner segments from the salamander retina. J Physiol. 1982; 331:253–284. [PubMed: 7153904]

Belgum JH, Copenhagen DR. Synaptic transfer of rod signals to horizontal and bipolar cells in the retina of the toad (*Bufo marinus*). J Physiol. 1988; 396:225–245. [PubMed: 3137327]

Berntson AK, Morgans CW. Distribution of the presynaptic calcium sensors, synaptotagmin I/II and synaptotagmin III, in the goldfish and rodent retinas. J Vis. 2003; 3:274–280. [PubMed: 12803536]

Berntson A, Taylor WR, Morgans CW. Molecular identity, synaptic localization, and physiology of calcium channels in retinal bipolar cells. J Neurosci Res. 2003; 71:146–151. [PubMed: 12478624]

Beutner D, Voets T, Neher E, Moser T. Calcium dependence of exocytosis and endocytosis at the cochlear inner hair cell afferent synapse. Neuron. 2001; 29:681–690. [PubMed: 11301027]

Bollmann JH, Sakmann B, Borst JG. Calcium sensitivity of glutamate release in a calyx-type terminal. Science. 2000; 289:953–957. [PubMed: 10937999]

Borst JGG, Sakmann B. Effect of changes in action potential shape on calcium currents and transmitter release in a calyx-type synapse of the rat auditory brainstem. Philos Trans R Soc Lond B Biol Sci. 1999; 354:347–355. [PubMed: 10212483]

Butz S, Fernandez-Chacon R, Schmitz F, Jahn R, Sudhof TC. The subcellular localizations of atypical synaptotagmins III and VI. Synaptotagmin III is enriched in synapses and synaptic plasma membranes but not in synaptic vesicles. J Biol Chem. 1999; 274:18290–18296. [PubMed: 10373432]

Chow RH, Klingauf J, Neher E. Time course of Ca^{2+} concentration triggering exocytosis in neuroendocrine cells. Proc Natl Acad Sci USA. 1994; 91:12765–12769. [PubMed: 7809118]

Corey DP, Dubinsky JM, Schwartz EA. The calcium current in inner segments of rods from the salamander (*Ambystoma tigrinum*) retina. J Physiol. 1984; 354:557–575. [PubMed: 6090654]

Dodge FA, Rahamimoff R. Co-operative action of calcium ions in transmitter release at the neuromuscular junction. J Physiol. 1967; 193:419–432. [PubMed: 6065887]

Donnelly DF. A novel method for rapid measurement of membrane resistance, capacitance, and access resistance. Biophys J. 1994; 66:873–877. [PubMed: 8011919]

Dunlap K, Luebke JI, Turner TJ. Exocytotic Ca^{2+} channels in mammalian central neurons. Trends Neurosci. 1995; 18:89–98. [PubMed: 7537420]

Gentet LJ, Stuart GJ, Clements JD. Direct measurement of specific membrane capacitance in neurons. Biophys J. 2000; 79:314–320. [PubMed: 10866957]

Geppert M, Goda Y, Hammer RE, Li C, Rosahl TW, Stevens CF, Sudhof TC. Synaptotagmin I: a major Ca^{2+} sensor for transmitter release at a central synapse. Cell. 1994; 79:717–727. [PubMed: 7954835]

Gillis, KD. Techniques for membrane capacitance measurements. In: Sakmann, B.; Neher, E., editors. Single-Channel Recordings. New York: Plenum Press; 1995. p. 155-198.

Grynkiewicz G, Poenie M, Tsien RY. A new generation of Ca^{2+} indicators with greatly improved fluorescence properties. J Biol Chem. 1985; 260:3440–3450. [PubMed: 3838314]

Heidelberger R. Adenosine triphosphate and the late steps in calcium-dependent exocytosis at a ribbon synapse. J Gen Physiol. 1998; 111:225–241. [PubMed: 9450941]

Heidelberger R. ATP is required at an early step in compensatory endocytosis in synaptic terminals. J Neurosci. 2001a; 21:6467–6474. [PubMed: 11517235]

Heidelberger R. Electrophysiological approaches to the study of neuronal exocytosis and synaptic vesicle dynamics. Rev Physiol Biochem Pharmacol. 2001b; 143:1–80. [PubMed: 11428263]

Heidelberger R, Matthews G. Calcium influx and calcium current in single synaptic terminals of goldfish retinal bipolar neurons. J Physiol. 1992; 447:235–256. [PubMed: 1317429]

Heidelberger R, Heinemann C, Neher E, Matthews G. Calcium dependence of the rate of exocytosis in a synaptic terminal. Nature. 1994; 371:513–515. [PubMed: 7935764]

Heidelberger R, Sterling P, Matthews G. Roles of ATP in depletion and replenishment of the releasable pool of synaptic vesicles. J Neurophysiol. 2002; 88:98–106. [PubMed: 12091535]

Heidelberger R, Wang MM, Sherry DM. Differential distribution of synaptotagmin immunoreactivity among synapses in the goldfish, salamander, and mouse retina. Vis Neurosci. 2003; 20:37–49. [PubMed: 12699082]

Heinemann C, Chow RH, Neher E, Zucker RS. Kinetics of the secretory response in bovine chromaffin cells following flash photolysis of caged Ca^{2+} Biophys J. 1994; 67:2546–2557. [PubMed: 7696493]

Helmchen F, Borst JG, Sakmann B. Calcium dynamics associated with a single action potential in a CNS presynaptic terminal. Biophys J. 1997; 72:1458–1471. [PubMed: 9138591]

Kim HG, Miller RF. Rods and cones activate different excitatory amino acid receptors on the mudpuppy retinal horizontal cell. Brain Res. 1991; 538:141–146. [PubMed: 1673359]

Kim HG, Miller RF. Properties of synaptic transmission from photoreceptors to bipolar cells in the mudpuppy retina. J Neurophysiol. 1993; 69:352–360. [PubMed: 8384660]

Kits KS, de Vlieger TA, Kooi BW, Mansvelder HD. Diffusion barriers limit the effect of mobile calcium buffers on exocytosis of large dense cored vesicles. Biophys J. 1999; 76:1693–1705. [PubMed: 10049349]

Kreft M, Krizaj D, Grilc S, Zorec R. Properties of exocytotic response in vertebrate photoreceptors. J Neurophysiol. 2003; 90:218–225. [PubMed: 12660355]

Kyrozis A, Reichling DB. Perforated-patch recording with gramicidin avoids artifactual changes in intracellular chloride concentration. J Neurosci Methods. 1995; 57:27–35. [PubMed: 7540702]

Lagnado L, Gomis A, Job C. Continuous vesicle cycling in the synaptic terminal of retinal bipolar cells. Neuron. 1996; 17:957–967. [PubMed: 8938127]

Lenzi D, von Gersdorff H. Structure suggests function: the case for synaptic ribbons as exocytotic nanomachines. Bioessays. 2001; 23:831–840. [PubMed: 11536295]

Lindau M, Neher E. Patch-clamp techniques for time-resolved capacitance measurements in single cells. Pflugers Arch. 1988; 411:137–146. [PubMed: 3357753]

Mennerick S, Matthews G. Ultrafast exocytosis elicited by calcium current in synaptic terminals of retinal bipolar neurons. Neuron. 1996; 17:1241–1249. [PubMed: 8982170]

Messler P, Harz H, Uhl R. Instrumentation for multi-wavelengths excitation imaging. J Neurosci Methods. 1996; 69:137–147. [PubMed: 8946316]

Mintz IM, Sabatini BL, Regehr WG. Calcium control of transmitter release at a cerebellar synapse. Neuron. 1995; 15:675–688. [PubMed: 7546746]

Morgans CW. Localization of the alpha(1F) calcium channel subunit in the rat retina. Invest Ophthalmol Vis Sci. 2001; 42:2414–2418. [PubMed: 11527958]

Morgans CW, El Far O, Berntson A, Wassle H, Taylor WR. Calcium extrusion from mammalian photoreceptor terminals. J Neurosci. 1998; 18:2467–2474. [PubMed: 9502807]

Moser T, Beutner D. Kinetics of exocytosis and endocytosis at the cochlear inner hair cell afferent synapse of the mouse. Proc Natl Acad Sci USA. 2000; 97:883–888. [PubMed: 10639174]

Nachman-Clewner M, St Jules R, Townes-Anderson E. L-type calcium channels in the photoreceptor ribbon synapse: localization and role in plasticity. J Comp Neurol. 1999; 415:1–16. [PubMed: 10540354]

Naka KI, Itoh MA, Chappell RL. Dynamics of turtle cones. J Gen Physiol. 1987; 89:321–337. [PubMed: 3559514]

Naraghi M, Muller TH, Neher E. Two-dimensional determination of the cellular Ca^{2+} binding in bovine chromaffin cells. Biophys J. 1998; 75:1635–1647. [PubMed: 9746506]

Neher E, Zucker RS. Multiple calcium-dependent processes related to secretion in bovine chromaffin cells. Neuron. 1993; 10:21–30. [PubMed: 8427700]

Parsons TD, Sterling P. Synaptic ribbon. Conveyor belt or safety belt? Neuron. 2003; 37:379–382. [PubMed: 12575947]

Parsons TD, Lenzi D, Almers W, Roberts WM. Calcium-triggered exocytosis and endocytosis in an isolated presynaptic cell: capacitance measurements in saccular hair cells. Neuron. 1994; 13:875–883. [PubMed: 7946334]

Pierantoni, RL.; McCann, GD. A quantitative study on synaptic ribbons in the photoreceptors of turtle and frog. In: Borsellino, A.; Cervetto, L., editors. Photoreceptors. New York: Plenum Press; 1981. p. 255-283.

Rabl K, Thoreson WB. Calcium-dependent inactivation and depletion of synaptic cleft calcium ions combine to regulate rod calcium currents under physiological conditions. Eur J Neurosci. 2002; 16:2070–2077. [PubMed: 12473074]

Raviola E, Gilula NB. Intramembrane organization of specialized contacts in the outer plexiform layer of the retina. A freeze-fracture study in monkeys and rabbits. J Cell Biol. 1975; 65:192–222. [PubMed: 1127010]

Rieke F, Schwartz E. Asynchronous transmitter release: control of exocytosis and endocytosis at the salamander rod synapse. J Physiol. 1996; 493:1–8. [PubMed: 8735690]

Roberts WM, Jacobs RA, Hudspeth AJ. Colocalization of ion channels involved in frequency selectivity and synaptic transmission at presynaptic active zones of hair cells. J Neurosci. 1990; 10:3664–3684. [PubMed: 1700083]

Rohlicek V, Schmid A. Dual-frequency method for synchronous measurement of cell capacitance, membrane conductance and access resistance on single cells. Pflugers Arch. 1994; 428:30–38. [PubMed: 7971159]

Rouze NC, Schwartz EA. Continuous and transient vesicle cycling at a ribbon synapse. J Neurosci. 1998; 18:8614–8624. [PubMed: 9786969]

Sakai HM, Naka K. Signal transmission in the catfish retina. V. Sensitivity and circuit. J Neurophysiol. 1987; 58:1329–1350. [PubMed: 2830371]

Schmitz Y, Witkovsky P. Dependence of photoreceptor glutamate release on a dihydropyridine-sensitive calcium channel. Neuroscience. 1997; 78:1209–1216. [PubMed: 9174087]

Schneggenburger R, Neher E. Intracellular calcium dependence of transmitter release rates at a fast central synapse. Nature. 2000; 406:889–893. [PubMed: 10972290]

Sun JY, Wu XS, Wu LG. Single and multiple vesicle fusion induce different rates of endocytosis at a central synapse. Nature. 2002; 417:555–559. [PubMed: 12037569]

Tatsuoka H, Reese TS. New structural features of synapses in the anteroventral cochlear nucleus prepared by direct freezing and freeze-substitution. J Comp Neurol. 1989; 290:343–357. [PubMed: 2592616]

Thoreson WB, Witkovsky P. Glutamate receptors and circuits in the vertebrate retina. Prog Retin Eye Res. 1999; 18:765–810. [PubMed: 10530751]

Thoreson WB, Tranchina D, Witkovsky P. Kinetics of synaptic transfer from rods and cones to horizontal cells in the salamander retina. Neuroscience. 2003; 122:785–798. [PubMed: 14622921]

Townes-Anderson E, MacLeish PR, Raviola E. Rod cells dissociated from mature salamander retina: ultrastructure and uptake of horseradish peroxidase. J Cell Biol. 1985; 100:175–188. [PubMed: 3965470]

Townes-Anderson E, Dacheux RF, Raviola E. Rod photoreceptors dissociated from the adult rabbit retina. J Neurosci. 1988; 8:320–331. [PubMed: 3339415]

Tranchina D, Gordon J, Shapley R, Toyoda J. Linear information processing in the retina: a study of horizontal cell responses. Proc Natl Acad Sci USA. 1981; 78:6540–6542. [PubMed: 6947242]

Ullrich B, Sudhof TC. Distribution of synaptic markers in the retina: implications for synaptic vesicle traffic in ribbon synapses. J Physiol (Paris). 1994; 88:249–257. [PubMed: 7874086]

Voets T. Dissection of three Ca^{2+}-dependent steps leading to secretion in chromaffin cells from mouse adrenal slices. Neuron. 2000; 28:537–545. [PubMed: 11144362]

von Gersdorff H, Matthews G. Dynamics of synaptic vesicle fusion and membrane retrieval in synaptic terminals. Nature. 1994a; 367:735–739. [PubMed: 7906397]

von Gersdorff H, Matthews G. Inhibition of endocytosis by elevated internal calcium in a synaptic terminal. Nature. 1994b; 370:652–655. [PubMed: 8065451]

von Gersdorff H, Vardi E, Matthews G, Sterling P. Evidence that vesicles on the synaptic ribbon of retinal bipolar neurons can be rapidly released. Neuron. 1996; 16:1221–1227. [PubMed: 8663998]

von Gersdorff H, Sakaba T, Berglund K, Tachibana M. Submillisecond kinetics of glutamate release from a sensory synapse. Neuron. 1998; 21:1177–1188. [PubMed: 9856472]

Witkovsky P, Schmitz Y, Akopian A, Krizaj D, Tranchina D. Gain of rod to horizontal cell synaptic transfer: relation to glutamate release and a dihydropyridine-sensitive calcium current. J Neurosci. 1997; 17:7297–7306. [PubMed: 9295376]

Wu SM. Synaptic transmission from rods to bipolar cells in the tiger salamander retina. Proc Natl Acad Sci USA. 1985; 82:3944–3947. [PubMed: 2987955]

Wu SM. Synaptic transmission from rods to horizontal cells in dark-adapted tiger salamander retina. Vision Res. 1988; 28:1–8. [PubMed: 2842959]

Wu LG, Westenbroek RE, Borst JG, Catterall WA, Sakmann B. Calcium channel types with distinct presynaptic localization couple differentially to transmitter release in single calyx-type synapses. J Neurosci. 1999; 19:726–736. [PubMed: 9880593]

Yang Y, Udayasankar S, Dunning J, Chen P, Gillis KD. A highly Ca^{2+}-sensitive pool of vesicles is regulated by protein kinase C in adrenal chromaffin cells. Proc Natl Acad Sci USA. 2002; 99:17060–17065. [PubMed: 12446844]

Zenisek D, Matthews G. The role of mitochondria in presynaptic calcium handling at a ribbon synapse. Neuron. 2000; 25:229–237. [PubMed: 10707986]

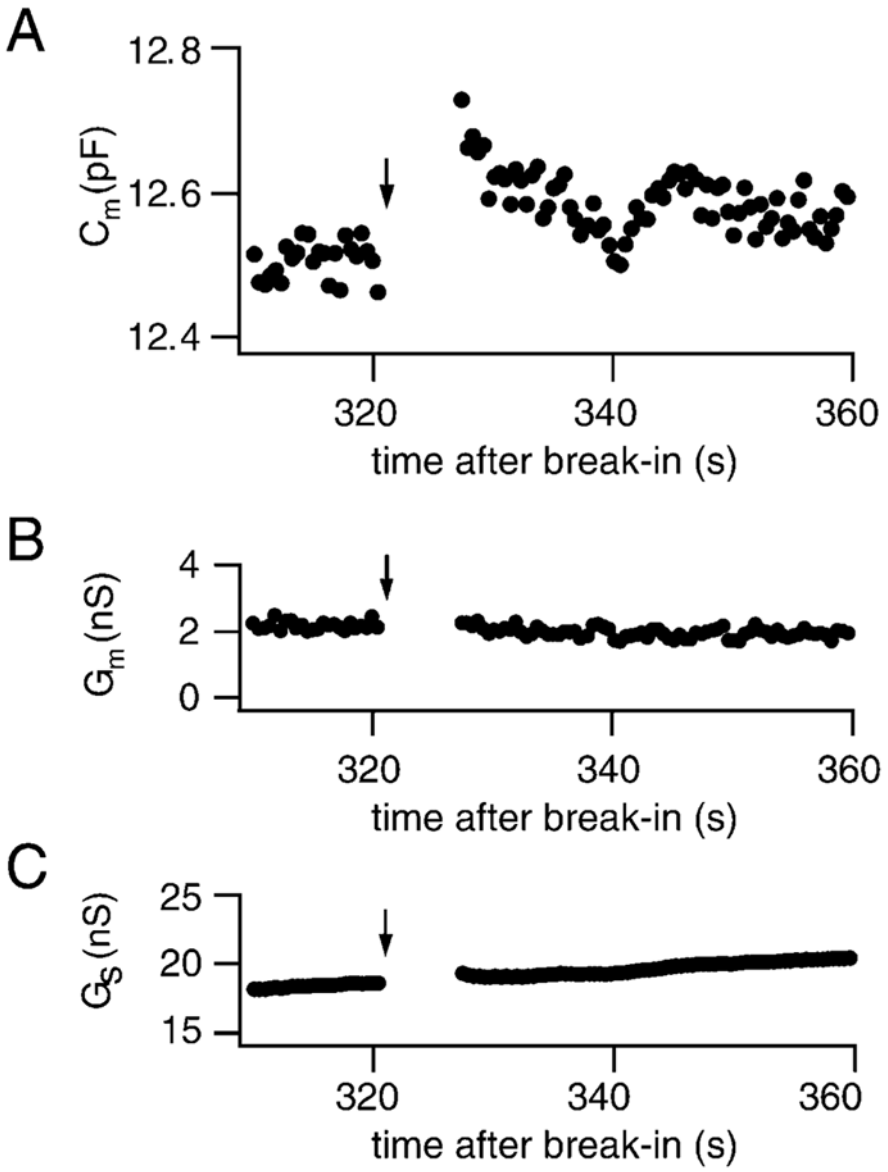

Figure 1. Depolarization Triggers Exocytosis in an Isolated Rod

(A) Capacitance increase evoked by a voltage step (−65 to −5 mV, 5 s) given at the arrow. No significant change in membrane or series conductance associated with the voltage step was observed (B and C).

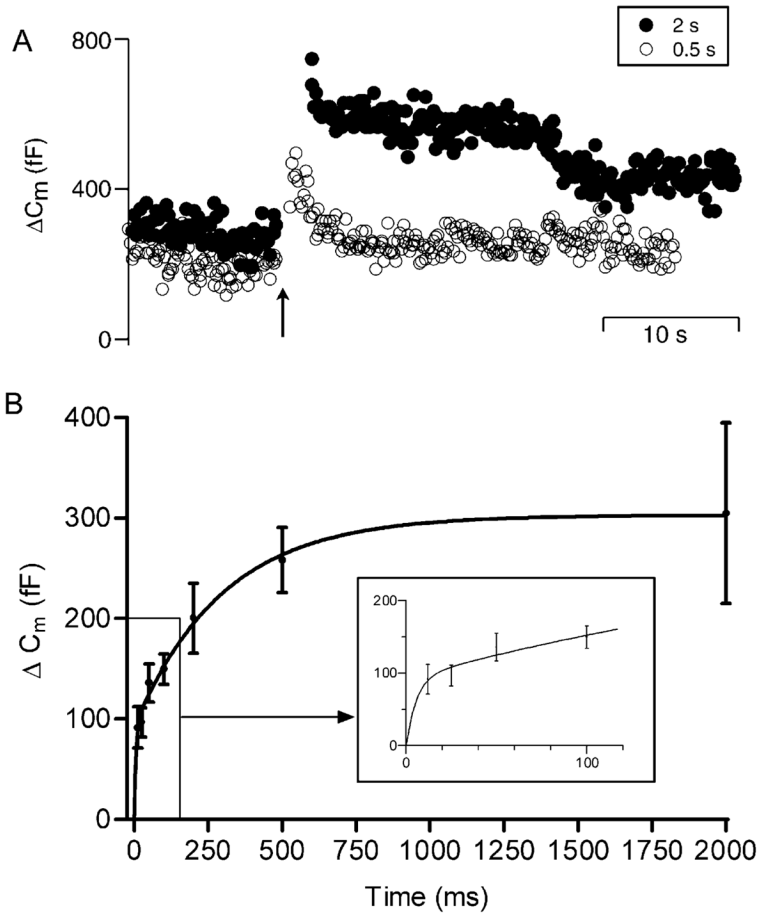

Figure 2. Pulse Duration Experiments Reveal Two Kinetic Components of Exocytosis in Rods

(A) Increasing the duration of a step depolarization (−65 to −5 mV) from 0.5 s (open circles) to 2 s (closed circles) increased the amplitude of the capacitance jump. Arrow indicates beginning of the voltage step.

(B) Depolarization-evoked capacitance increase plotted as a function of step duration. The capacitance/duration relation was fit with a dual exponential (τ_1 = 5.6 ms, amplitude$_1$ = 92.4 fF; τ_2 = 298 ms, amplitude$_2$ = 210.4 fF). Sample sizes: 12 ms, n = 50; 25 ms, n = 42; 50 ms, n = 43; 100 ms, n = 66; 200 ms, n = 46; 500 ms, n = 45; 2 s, n = 41. Inset magnifies the initial fast rise in capacitance.

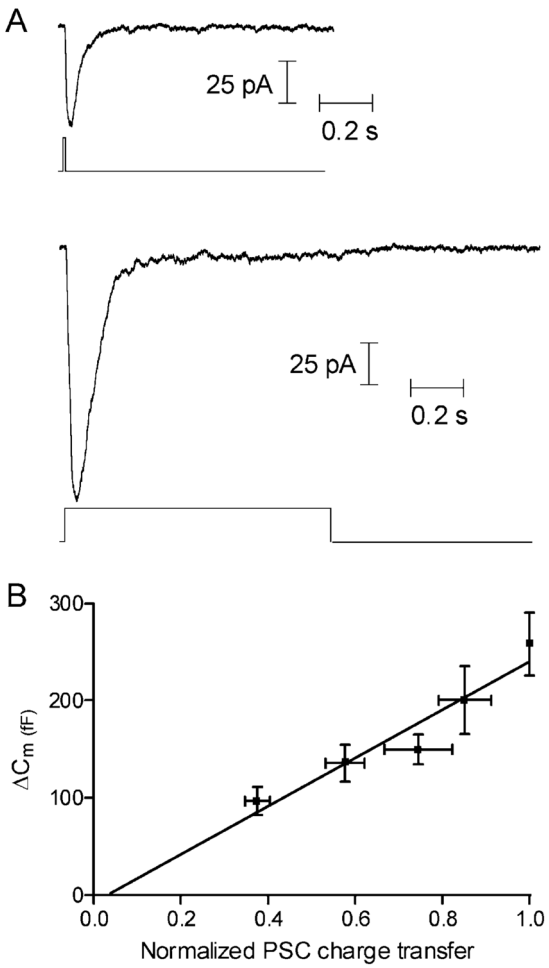

Figure 3. The Capacitance Jump Accurately Reports Neurotransmitter Release

(A) Increasing the duration of a depolarizing step (−70 to −10 mV) applied to a rod from 10 ms (top trace) to 1.0 s (lower trace) increased the amplitude of the PSC evoked in a postsynaptic OFF bipolar cell.

(B) PSC charge transfer, obtained from paired pre- and postsynaptic recordings, was linearly related to the capacitance increase evoked by depolarizing steps of the same duration (25, 50, 100, 200, and 500 ms; $r^2 = 0.92$). Charge transfer was normalized to the charge transfer evoked by a 500 ms step. PSC data in (A) and (B) were obtained in the presence of cyclothiazide (0.1 mM) and were from 2 horizontal cells and 4 OFF bipolar cells. Capacitance data are taken from the experiments shown in Figure 2.

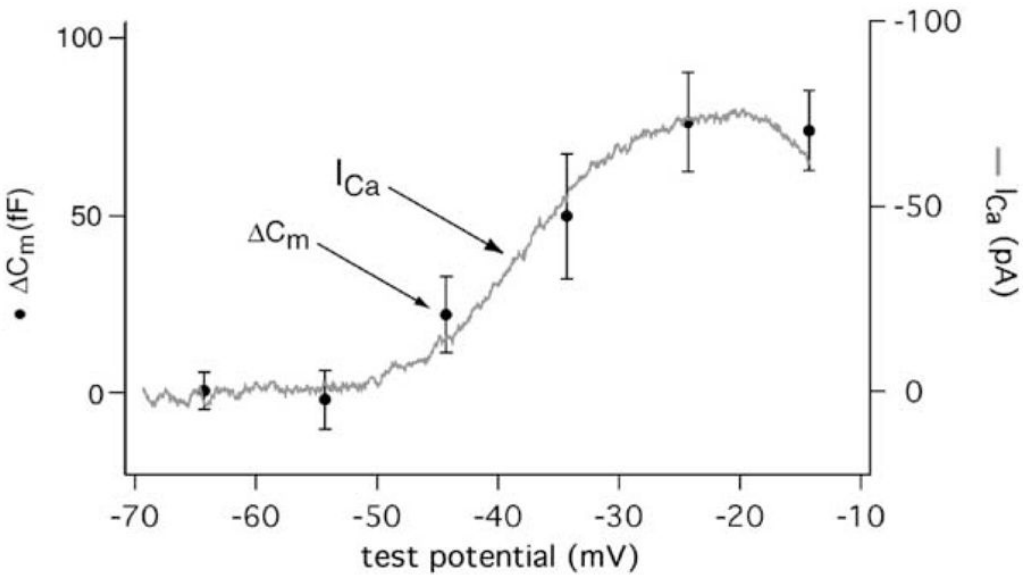

Figure 4. The Voltage Dependence of Depolarization-Evoked Capacitance Increases Matches the Voltage Dependence of I_{Ca}

The amplitude of the capacitance jump evoked by a 100 ms step from a holding potential of −65 to a test potential is plotted against the test potential (left axis, circles, n = 11). The magnitude of exocytosis shows a sigmoidal relationship to voltage similar to I_{Ca} (right axis, data trace). I_{Ca} was recorded using ruptured patch recording techniques from isolated rods and evoked with a ramp depolarization (0.5 mV/ms, −90 to +60 mV). 1.8 mM Ca^{2+} was the charge carrier. K^+ channels were blocked with Cs^+ in the pipette and TEA in both the pipette and bathing solutions. Niflumic acid (0.1 mM) was added to inhibit Ca^{2+}-activated Cl^- channels. The same pipette solution was used in measuring both I_{Ca} and capacitance. I_{Ca} from 7 cells were normalized to 100 pA and then averaged to yield the current/voltage relationship shown.

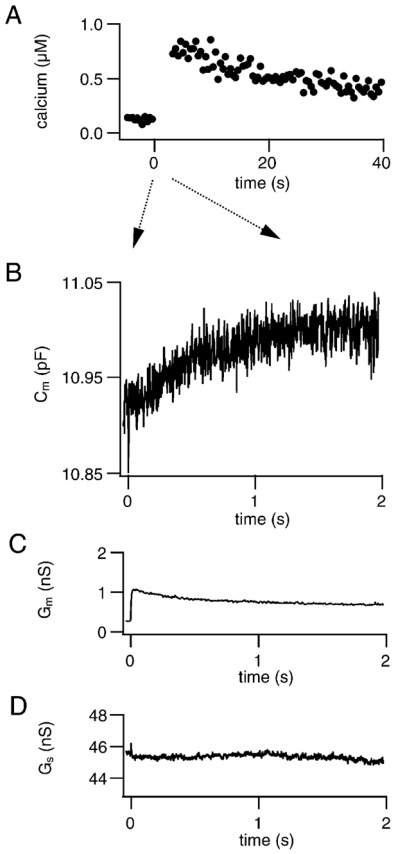

Figure 5. Exocytosis Was Triggered by the Elevation of Ca^{2+} to Submicromolar Levels by Flash Photolysis of Caged Ca^{2+}

(A) Flash photolysis of Ca^{2+}-loaded DM-nitrophen produced a rapid and spatially homogenous elevation of $[Ca^{2+}]_i$ in the rod synaptic terminal to 780 nM. $[Ca^{2+}]_i$ was measured with the low-affinity Ca^{2+} indicator dye Fura-FF.

(B–D) High-resolution traces show that the increase in $[Ca^{2+}]_i$ triggered a slowly developing increase in membrane capacitance (B) and an uncorrelated rapid increase in membrane conductance (C). No change in access resistance was observed (D). Note the difference in time scales between (A) and (B)–(D). For all panels, the UV flash is given at time = 0.

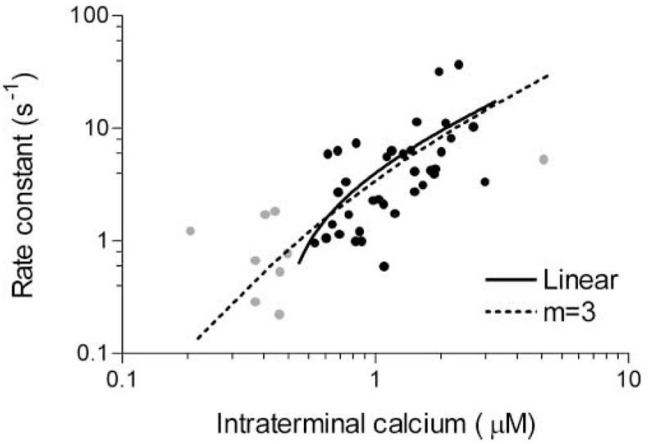

Figure 6. The Relationship between the Rate of Membrane Addition and $[Ca^{2+}]_i$ Is Approximately Linear within a Restricted Range of Physiological $[Ca^{2+}]_i$

Exponential rate constants, derived from a single exponential fit to the rising phase of each capacitance response evoked by the flash photolysis of caged Ca^{2+}, are plotted against the intraterminal $[Ca^{2+}]$ measured immediately after the flash (n = 45). Data points in the Ca^{2+} range from 0.5 to 3 μM (Rieke and Schwartz, 1996) are shown in black (n = 36); data points outside this range are shown in gray. Rate constants in the physiological Ca^{2+} range show a nearly linear relationship with Ca^{2+} as illustrated by the linear regression (solid line, slope = 6.70 ± 2.10, Y intercept = −2.72 ± 2.90, r^2 = 0.23). Across the entire range, the data could be simulated (dashed line) using a mathematical model of exocytosis that assumes three independent Ca^{2+} binding reactions followed by a final, Ca^{2+}-independent fusion step (see Experimental Procedures; also Heinemann et al., 1994; Voets, 2000).

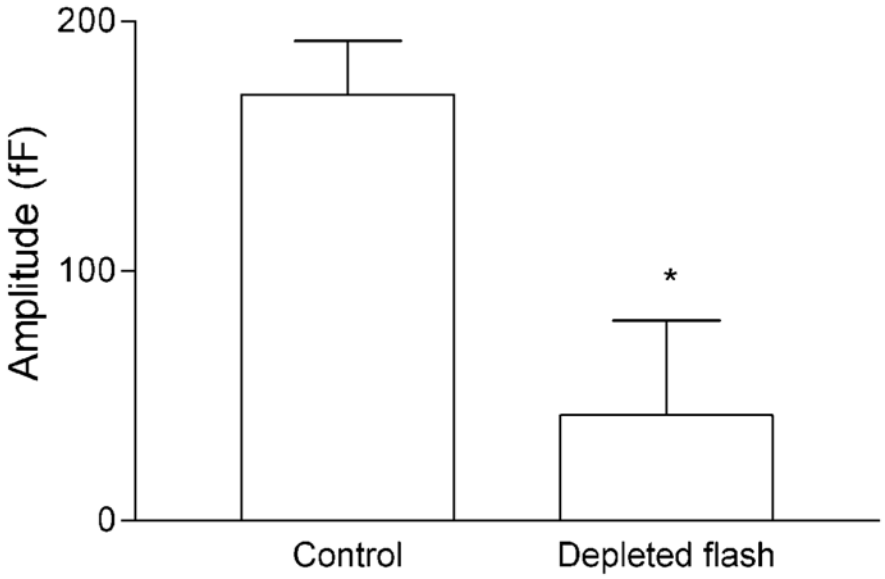

Figure 7. Vesicles that Exocytose in Response to Flash Photolysis of Caged Ca^{2+} also Fuse in Response to Ca^{2+} Influx through Voltage-Gated Channels

Bar graph compares the mean amplitude of the capacitance response evoked by a maximal intensity flash in control cells (170.7 ± 21.5 fF, n = 45) with the mean capacitance response evoked by the identical flash in cells in which the releasable pool was predepleted by a 2 s depolarization from −65 to −5 mV (42.2 ± 38.0 fF, n = 7). Prior depletion of the releasable pool significantly reduced the response to a flash relative to control (p = 0.03).

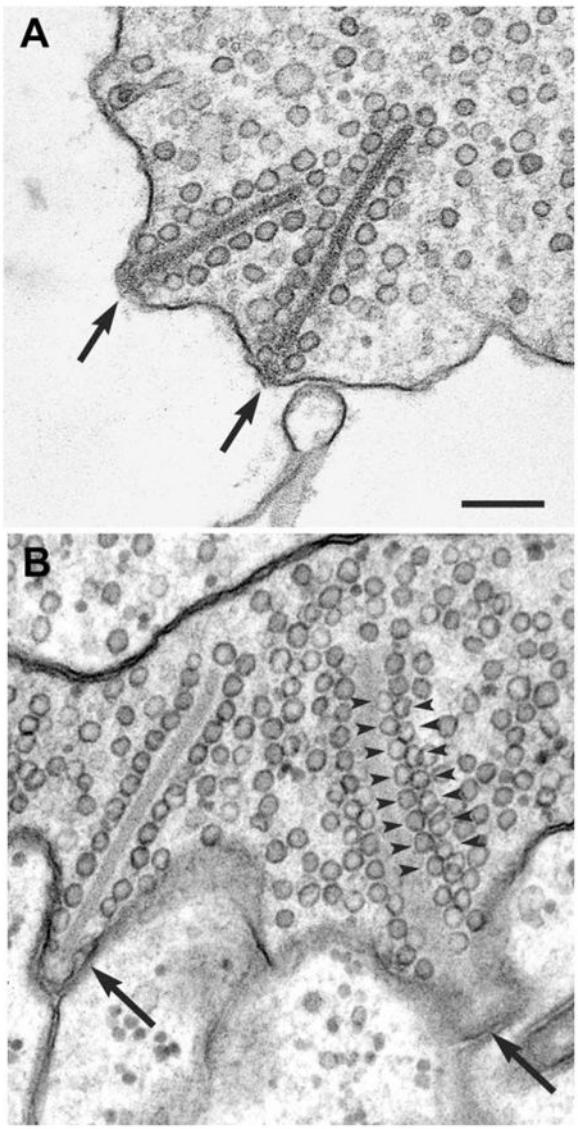

Figure 8. For Ultrastructural Analysis of Vesicle Pools that May Participate in Release, the Size of Ribbons, Number of Vesicles Tethered to the Presynaptic Ribbon, and the Diameter of Vesicles Were Determined by Examining Serially and Randomly Sectioned Rod Terminals

Ribbon-style active zones in isolated cells (A) are similar to those in the intact retina (B). Ribbons (arrows) are surrounded by vesicles and attached at a perpendicular angle to the membrane. In the retina, membrane-attached ribbons (arrows) are present opposite postsynaptic processes (B). At the far right of (B), a tangentially sectioned ribbon shows the hexagonal packing of tethered vesicles (arrowheads). Same magnification in (A) and (B). Bar = 200 nm.